1968

Effects of pressure on the mechanical properties of magnesium

Joseph George Hoeg

EFFECTS OF PRESSURE ON THE MECHANICAL PROPERTIES OF MAGNESIUM

BY

JOSEPH GEORGE HOEG, 1943

A

THESIS

submitted to the faculty of

THE UNIVERSITY OF MISSOURI AT ROLLA

in partial fulfillment of the requirements for the

Degree of

MASTER OF SCIENCE IN ENGINEERING MECHANICS

Rolla, Missouri

1968

Approved by

Robert L. Davis (advisor) Peter G. Hansen

T. F. Lilienhoff R. F. Dawson

ABSTRACT

The data collected in an attempt to evaluate the pressure dependency of the mechanical properties of extruded AZ31B-F magnesium alloy are presented herein. This information was compiled from the results of compression tests run in hydraulic fluid environments pressurized to 50,000 psi, and tension tests run in the atmosphere. Specimen axial load and longitudinal strain were recorded and converted to effective stress and effective strain parameters for presentation.

The term pressure is defined, in this report, as the negative average of the principal stresses or, essentially, the negative of the hydrostatic component of stress. The effective stress and strain, at yield and fracture, which were achieved at various hydrostatic stress levels are plotted against the hydrostatic stress levels at which they occurred. It has been shown that the strength and ductility of this extruded alloy, measured at fracture, are increased by an increase in the hydrostatic stress component that exists at the time of fracture. In addition, the effective stress, at yield, is increased and the effective strain is decreased by an increase in the current pressure. An exception to the above seems to be the effective stress achieved at yield in uniaxial tension which is substantially greater than the highest effective yield stress obtained in compression at any fluid environment pressure. This anomaly is due to the fact that the specimen material was cold formed.

The aforementioned graphs are combined to form a three dimensional

yield and fracture model based on the parameters of effective stress, effective strain and pressure. This model shows the pressure dependent properties of the particular magnesium alloy under investigation. It is, however, incomplete since bi-axial tension tests run at various fluid pressure environments are needed to better define the tensile pressure region of the model, and compression tests conducted in higher fluid pressure environments are needed to determine the pressures required to obtain infinite ductility.

PREFACE

This report contains the results of research conducted in partial fulfillment of the requirements for the degree of Master of Science in Engineering Mechanics. The work was done in the Department of Engineering Mechanics at the University of Missouri at Rolla, under the direction of Dr. Robert L. Davis.

The author would like to take this opportunity to thank the individuals and organizations who made this work possible. Among these are the Carpenter Steel Company which provided the alloy steels used to machine the hardware; Messrs. Warren Krumke, Chief Machinist at the United States Naval Air Test Center Flight Test Division, and Marvin Vogler, of the Department of Engineering Mechanics, who constructed much of the hardware; the United States Department of the Interior Bureau of Mines which provided heat treatment facilities; and the Dow Chemical Company which supplied the magnesium alloy specimen material. Without the strong support of these people, this project would never have been completed.

Finally, I would like to extend my greatest appreciation to Dr. Davis for his guidance and encouragement.

TABLE OF CONTENTS

LIST OF ILLUSTRATIONS

Figures Page

SCOPE

It is the purpose of this thesis to:

(1) Investigate the effects of pressure on the mechanical properties of extruded AZ31B-F magnesium alloy.

(2) Illustrate the results in a yield and fracture model utilizing the parameters of effective stress ($\bar{\sigma}$), effective strain ($\bar{\varepsilon}$), and pressure (P).

I. INTRODUCTION

Most yield and fracture theories which enjoy widespread use in the engineering disciplines completely neglect the effect of the hydrostatic component of stress in specifying yield and fracture conditions. Besides the intuitive deduction that a material cannot sustain infinite hydrostatic tension, data is becoming available in quantities sufficient to point out possible inadequacies in these existing yield and fracture models. Essentially, what has been shown so far is that some materials yield at effective stress and effective strain levels that vary as some function of the spherical or hydrostatic component of stress that exists at yield. Similar observations have been made at fracture. In some materials, the effective stress and effective strain at fracture have been shown to increase with the hydrostatic stress component, thus indicating an increase in strength and ductility under such conditions. Pressure, a term which will be used herein to mean the negative hydrostatic component of stress, can also cause changes in the fracture mode in many materials. The general trend is that ductile failure occurs in compressive pressure environments and brittle failure in tensile pressure environments.

Not all materials show such a pressure dependency and, as a consequence, the task of formulating a yield and fracture criterion that will account for pressure effects and apply to large groups of materials will be exceedingly complex. Such a yield and fracture criterion will, no doubt, involve the use of parameters that are commonly associated with the microscopic aspects of materials science. However, as an expedient, it should be possible to formulate a yield and fracture model for groups of materials that behave similarly under pressure without recourse to such aforementioned parameters. These models are vital to the design of structural elements that must adhere to certain weight and size optimization guidelines. In these cases, large factors of safety are not appropriate, and the result may be the failure of the element if variation in material properties with pressure is neglected.

Essential to the existence of accurate yield and fracture theories is the availability of data accumulated from various combined loading experiments. This thesis embodies the results of an attempt to evaluate the pressure dependency of the mechanical properties of a particular magnesium alloy. To partially accomplish this objective, compression tests were run on 3 inch long, one inch diameter, cylindrical test specimens made from extruded AZ31B-F magnesium alloy while the specimens were submerged in a pressurized fluid environment. The resulting data, in addition to data from tension tests run in the atmosphere, were used to generate a pressure dependent yield and fracture model.

II. REVIEW OF LITERATURE

An extensive literature survey conducted in the Library of Congress by the author has shown that few people have investigated the effects of pressure on the mechanical properties of any material. Such work, as limited as it is, was largely initiated by Dr. P. W. Bridgman over forty years ago, and it was Bridgman who carried this field into the 1950's.

Early work by Cook[1], although crude, served to show that springs made of mild steel and electrolytic copper became more ductile in a high pressure fluid environment. Bridgman[2] reported on all tensile and compressive tests run in pressurized fluid environments by anyone prior to 1950 and commented that almost no work had been done in the area to that date. In this collection of data, no work on polycrystalline aggregates of magnesium or its alloys was described. Bridgman[3] investigated the compressibility of a single crystal of pure magnesium and reported that no discontinuities were observed in the compressibility curve. Beyond this, nothing has been done with magnesium or its alloys in the area that this thesis treats. This is born out by the recent bibliographical works of Zeitlin[4], Bundy et al[5], Bradley[6], Giardini and Lloyd[7], and the International Conference on the Physics of Solids at High Pressures[8].

Although interest in high pressure phenomena is increasing, a great deal of the recent work deals with microscopic effects rather than effects on a continuum. The only recent, noteworthy work dealing with the effects of pressure on a continuum was accomplished by Hu[9]. In this paper, Hu documents the results of experiments, similar to those described herein, which were performed on a particular type of brass. It is this report by Hu that gives substantial impetus to what has been suspected for some time concerning the dependence of ductility and other mechanical properties on pressure.

In short, there is no detailed information available on the effects of pressure on the mechanical properties of magnesium alloys. However, the works of Bridgman and Hu provide fragmentary data for some materials that show pressure to be factor in determining material properties. This alone, demands the investigation of these effects on all engineering materials.

III. INSTRUMENTATION

The most difficult instrumentation problem encountered in this research program was that of measuring relatively large strains in a specimen surrounded by high fluid pressure. Although the magnesium alloy from which the specimens were made was very brittle, longitudinal strains at fracture of 15 per-cent were anticipated. Under these circumstances, it was necessary to use post yield strain gauges with an appropriate high elongation cement. No data is available from the gauge manufacturers on the use of high elongation strain gauges in pressurized hydraulic fluid environments; but, the recommendations of Tien and Gordon[10] led to the selection of a constantan foil, epoxy backed, encapsulated, gauge with a one-fourth inch grid length (Budd EHE-141). These gauges are reported to have gauge factors which are unaffected by fluid environments up to approximately 60,000 psi.

A two component epoxy bonding agent was used to mount the strain gauges on the specimens. This cement (Budd GA-2) can sustain strains of over 15 per-cent and had been tested by the manufacturers[11] in fluid environments pressurized to levels beyond those encountered in these tests. The gauge installations were coated with 12 layers of nitrile rubber oil-proofing compound (Budd GW-2). Removal of this oil-proofing from the gauges on selected fractured specimens showed the compound to have excellent oil protection qualities.

A Budd P-350 strain indicator was used to read strains. Although a dummy specimen was used for temperature compensation, this was largely unnecessary since all equipment was soaked at room temperature for an extended period of time before each test, and variations in room temperature were less than 5 degrees Fahrenheit during each test. Also, the energy input into the hydraulic fluid during pressurization could result in a fluid temperature rise of only one degree Fahrenheit. Prior to each test, the fluid environment was pressure cycled several times to check for large zero shifts in indicated strain on return to ambient pressure. In the worst case, a 10 microinch/inch shift was experienced on the first cycling and, on successive cycles, the zero shifts were substantially less than this value.

The measurement of the axial stress superposed on the specimen by the ram was facilitated by the fact that the specimen did not undergo any large local changes in cross-sectional area or geometry during the test. Consequently, the axial stress due to the ram load was taken to be the load on the specimen divided by the current area. The load on the specimen is the total ram load minus the seal-friction drag and the pressure force due to the pressurized fluid. The combined drag force and pressure force was determined for each test run by adjusting the loading head speed to match the nominal speed used during the test, and then noting the force required to move the ram into the vessel. This force was monitored prior to each test at a time when the loading head was not yet in contact with the specimen.

The fluid pressure in the test vessel was measured with a helical Bourdon tube pressure gauge (Astraguage W-100-F). This gauge was calibrated by the manufacturers before shipment and was reported to be within 0.25 per-cent of the indicated pressure. No further calibration was attempted.

IV. DESCRIPTION OF APPARATUS

As mentioned previously, the specimens used for the compression tests were 3 inches long and one inch in diameter. This length/diameter ratio was selected in accordance with the ASTM specifications for compression tests of metals. The compression specimens were positioned within a thick-walled cylindrical pressure vessel, and an axial load was applied to the specimen via a ram which protruded from one of the vessel end-plugs. Since the ram diameter was smaller than that of the specimen, an adapter was fitted to the end of the ram to distribute the ram load evenly over the top surface of the specimen. Positioning of the specimen within the vessel was accomplished by using a one-eighth inch thick nylon washer with flexible internal splines as shown in Figure (1). This washer insured concentricity of the specimen and loading ram, while not generating any appreciable radial restraining forces. The vessel was placed vertically in a Tinius-Olsen Universal 200,000 pound testing machine. Fluid pressure was developed by a hand-operated pump (AMINCO 46-12180). A picture of a simulated hardware set-up is shown in Figure (2).

The vessel closures were threaded cylindrical plugs, and are shown with the internal vessel hardware in Figure (3). The lower end-plug was drilled and counterbored to accomodate two electrical leads for the strain gauges used on the specimen. The details of this installation are shown in Figure (4). Only rigid resin materials are suitable for the cone shaped insulator for the copper connectors. Soft insulators tend to extrude out of the annular space between the

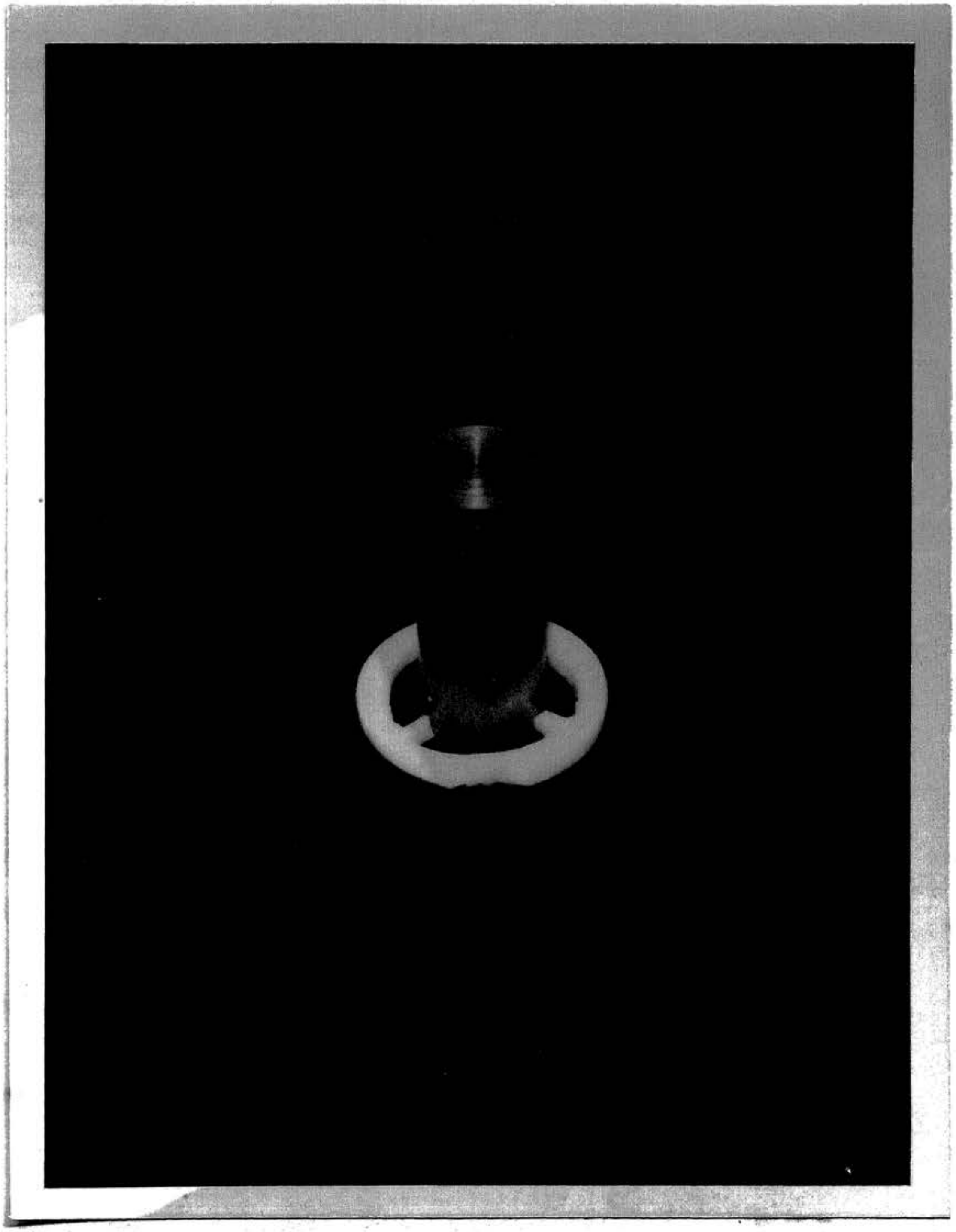

FIGURE (1) - SPECIMEN WITH ALIGNING WASHER

FIGURE (2) - SIMULATED HARDWARE SET-UP

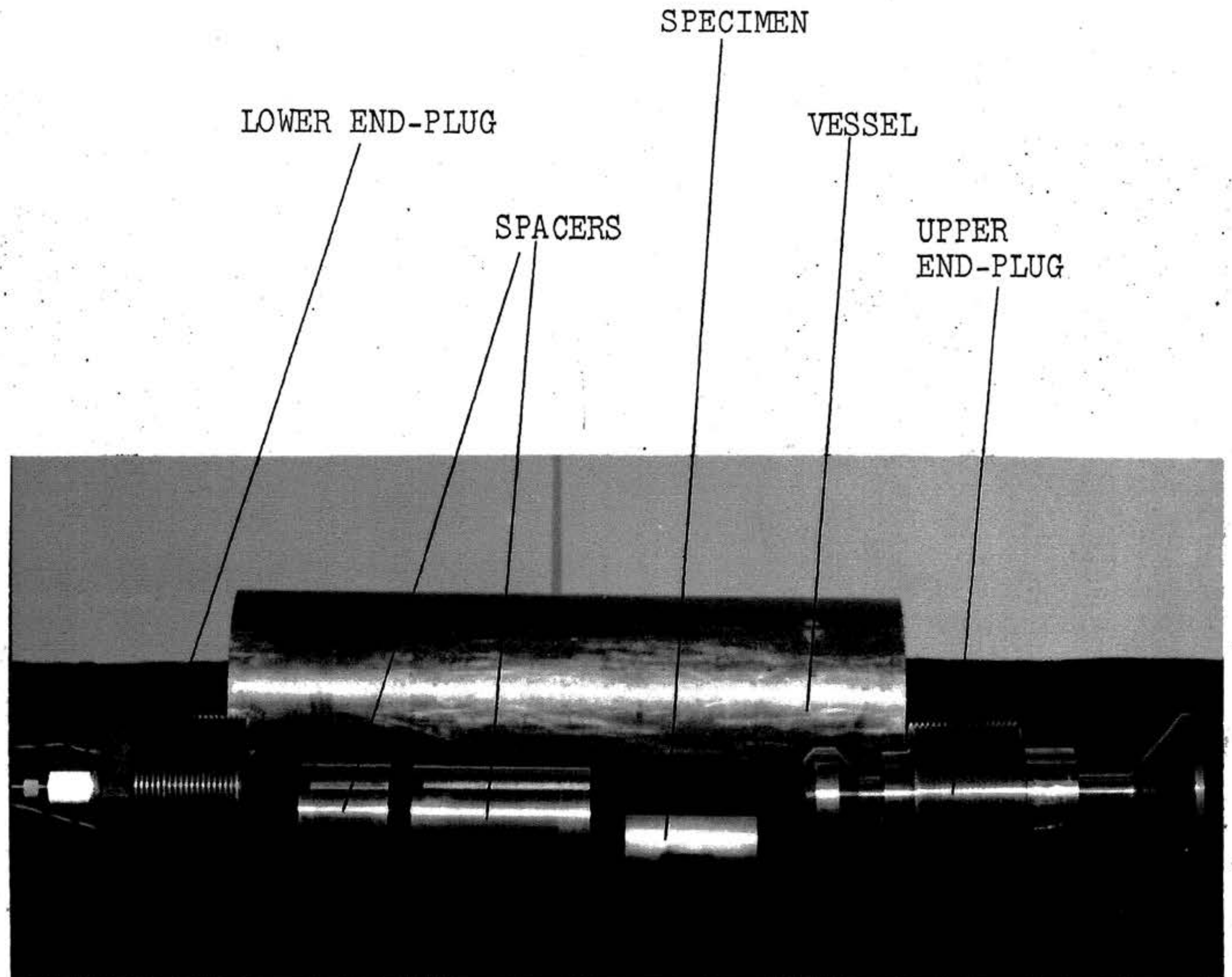

FIGURE (3) - EXPLODED VIEW OF INTERNAL VESSEL PARTS

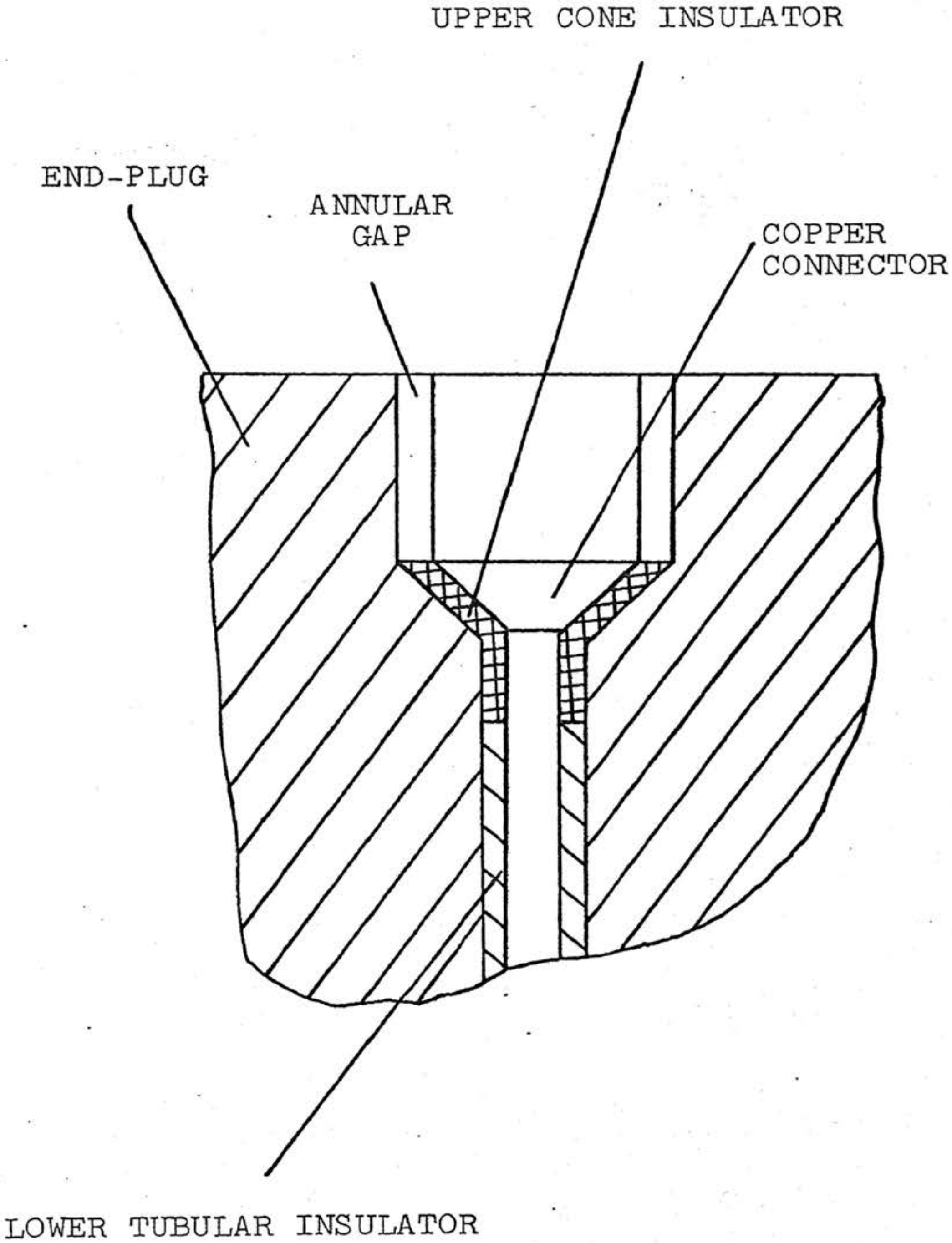

FIGURE (4) - END-PLUG ELECTRICAL LEAD

connector and the bored hole. In addition the lower end-plug contained a concentric hole and adapter to accomodate the one-fourth inch standard high pressure tubing from the hydraulic pump.

The upper end-plug containing the ram and seal subassembly is shown in Figure (5). The seal wafer with integral O-ring seats is illustrated in Figure (6). The seal wafer is made of DELRIN AF which is an acetate-filled flourocarbon resin. Use of this material resulted in extremely low seal friction drag forces on the moving ram and excellent anti-extrusion qualities. The clearance between the ram and the end-plug body was held to 0.0015-inch on the radius to minimize the tendency for the seal to extrude out through the annular region between the ram and the end-plug. This shallow clearance allowed a ram load of not more than 95,000 pounds. Beyond this, there would occur interference because of the Poisson effect. In order to obtain the greatest elastic strength possible in the ram, a maraging steel (Carpenter Ni MARK 300) with a yield strength in excess of 300,000 psi was selected. The ram was polished to a surface finish of 64 microinches root-mean-square to achieve a satisfactory sealing surface.

At low pressures, the O-rings seal the fluid and the DELRIN AF wafer acts as an anti-extrusion carrier; and, at higher pressures, the DELRIN AF wafer itself deforms into a seal. The fit between the wafer and the ram is 0.002-inch on the radius; and, as a consequence, no extrusion problems were encountered with the use of O-rings. Nitrile rubber O-rings were selected since they are inert when exposed to the

FIGURE (5) - UPPER END-PLUG AND RAM SEAL

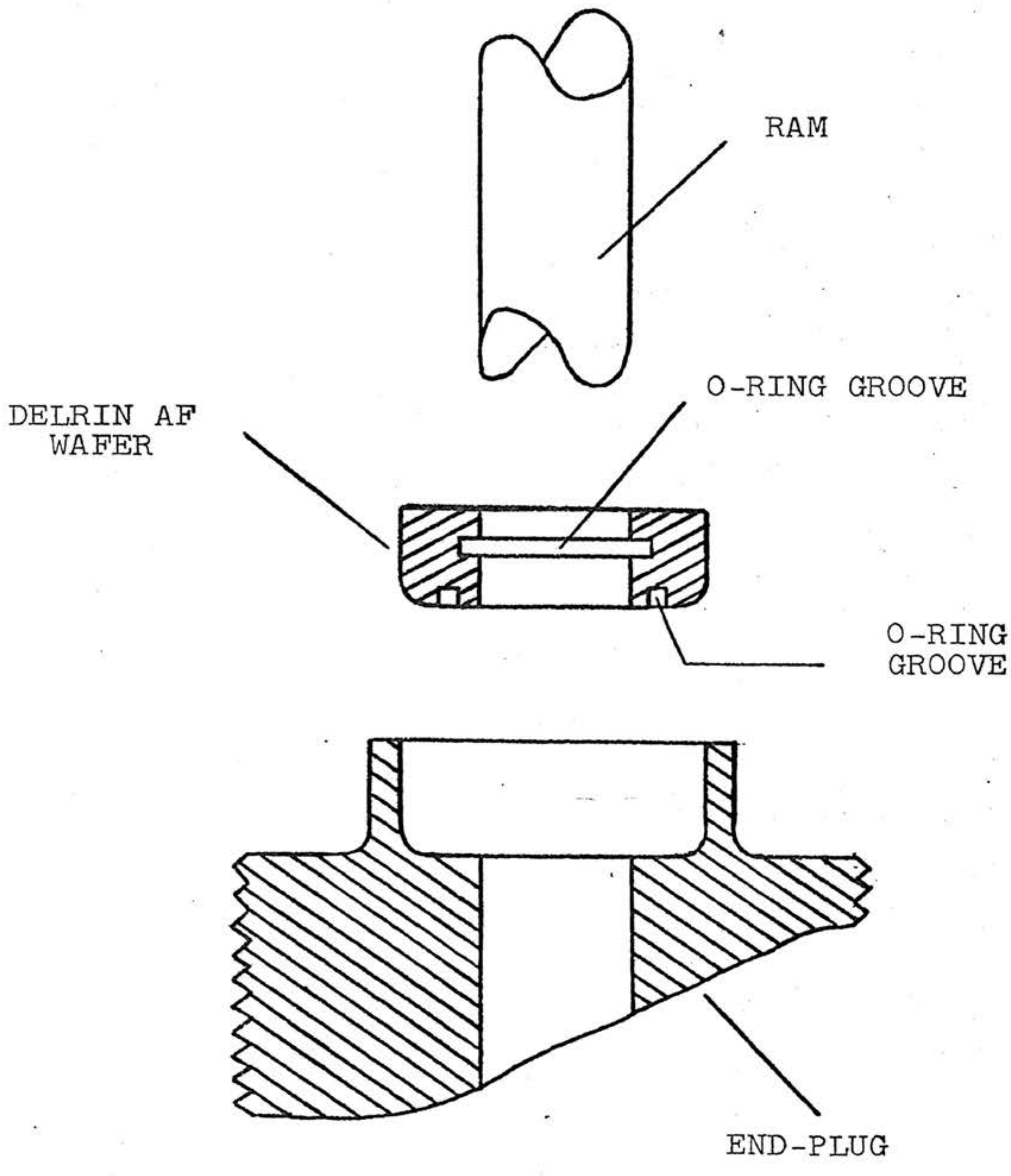

FIGURE (6) - UPPER END-PLUG AND RAM SEAL
SCHEMATIC

the pressurizing medium (MIL-6083B hydraulic fluid).

Two different types of seals were used to seal the end-plug against the mating vessel surface. The lower end-plug was sealed with an ordinary nitrile rubber O-ring supported by a brass anti-extrusion back-up ring. This seal arrangement is illustrated in Figure (7). The top end-plug was sealed with a silver plated Inconel-X C-ring (Pressure Science Inc. 10111-32) as shown in Figure (8). The seal seat surfaces for these C-rings must have at least a 64 microinch root-mean-square surface finish. All seals used performed flawlessly to pressures of 50,000 psi.

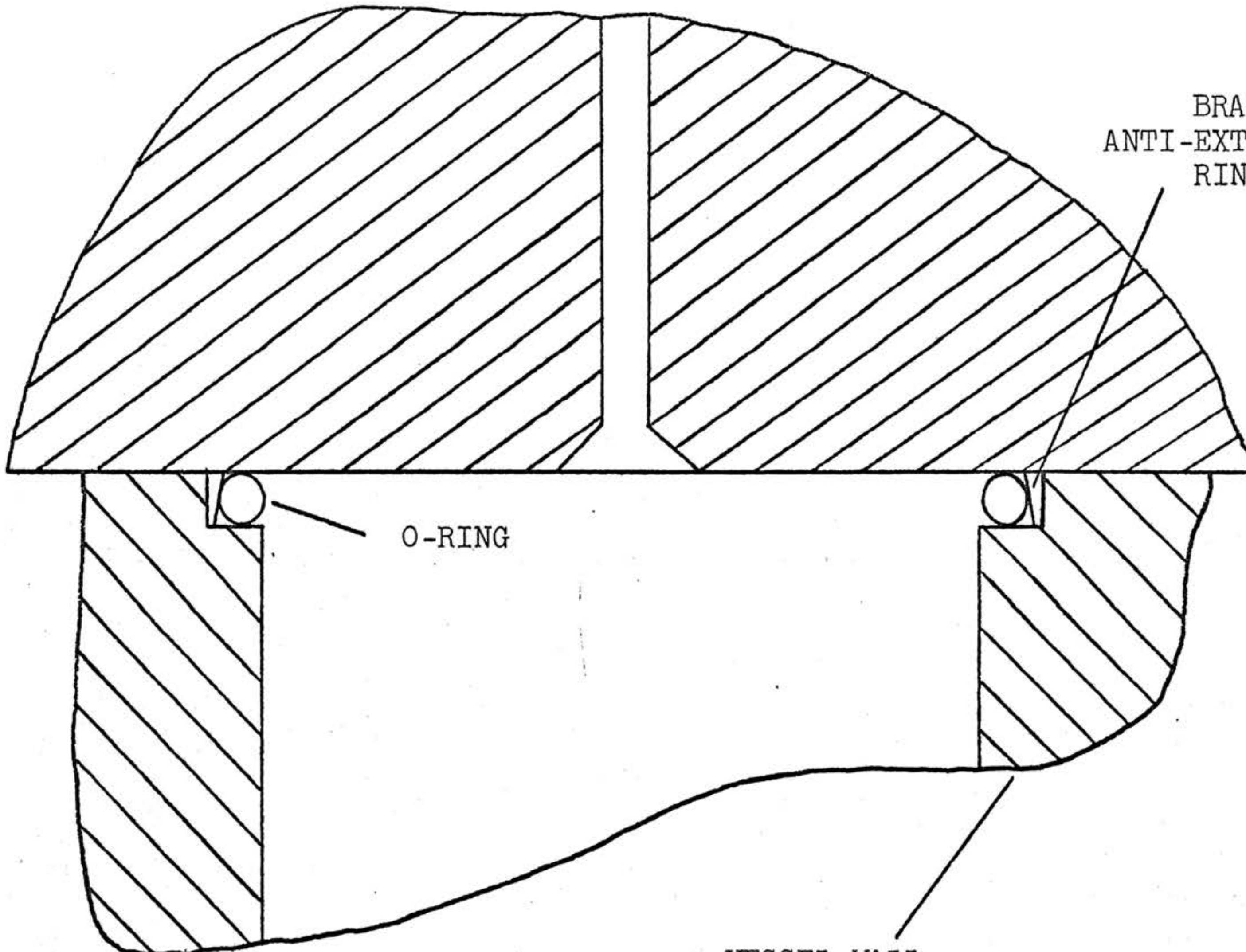

FIGURE (7) - LOWER END-PLUG SEAL

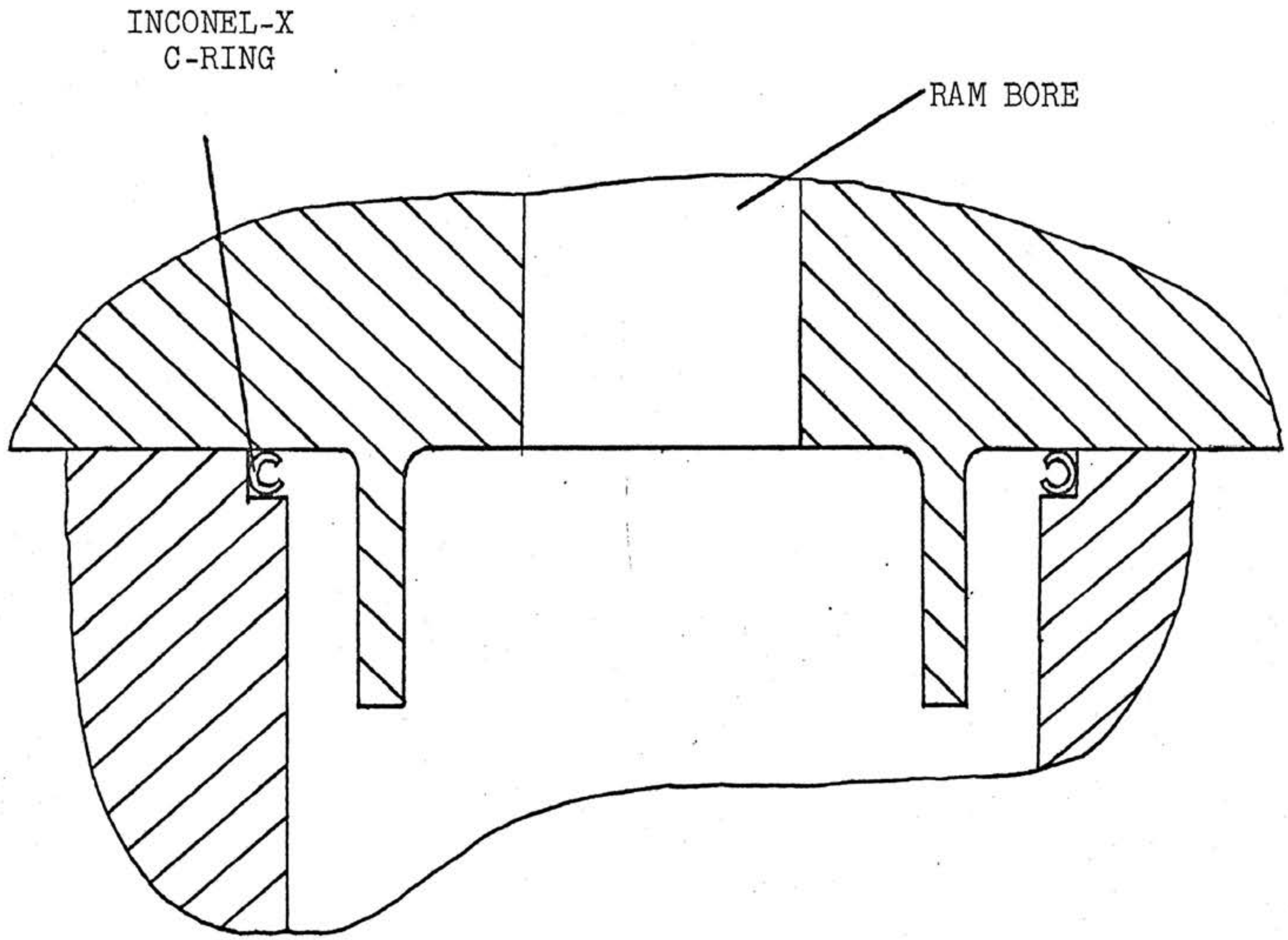

FIGURE (8) - UPPER END-PLUG SEAL

V. DISCUSSION

The ram load and longitudinal strain values for the six compression tests, and the axial specimen load and the longitudinal strain values for the tension test are tabulated in Appendix A. Although it was not possible to maintain a constant strain rate throughout each test, the strain rate varied within the range from 3 to 20 microinches/inch-second which is sufficiently slow to eliminate strain rate effects. The resulting data are presented in terms of effective stress versus pressure plots, effective strain versus pressure plots, and a three dimensional yield and fracture model involving effective stress, effective strain, and pressure.

Effective stress and effective strain, which represent stress and strain vectors in a deviatoric plane, have been chosen as display parameters because all principal stresses and strains are manifest, respectively, in these quantities. The effective stress is defined as

$$\bar{\sigma} = \{(\sigma_1-\sigma_2)^2+(\sigma_2-\sigma_3)^2+(\sigma_3-\sigma_1)^2\}^{.5}/\sqrt{2} \qquad (1)$$

where σ_1, σ_2, and σ_3 are the three principal stresses. Similarly, effective strain is defined as

$$\bar{\varepsilon} = \{(\varepsilon_1-\varepsilon_2)^2+(\varepsilon_2-\varepsilon_3)^2+(\varepsilon_3-\varepsilon_1)^2\}^{.5} \times \sqrt{2}/3 \qquad (2)$$

where ε_1, ε_2, and ε_3 are the principal strains. For the case considered here, the effective stress is simply equal to the longitudinal stress generated by the ram, since the superposed fluid pressure does not affect the principal stress differences. Also, the effective strain definition reduces to

$$\bar{\varepsilon} = 2(1+\nu)\varepsilon_1/3 \qquad (3)$$

where ε_1 is the longitudinal strain and ν is Poisson's ratio. As long as the specimen remains elastic, $\bar{\varepsilon} = .9\varepsilon_1$; since, Poisson's ratio is 0.35 in the elastic region for this material. When Poisson's ratio begins the transition to 0.50, its plastic value, expression (2) must be used in incremental form.

As the specimen was strained into the plastic region, an increment of effective strain was computed using the current average value for Poisson's ratio, and this increment was then added to the total effective strain up to that point. The assumed Poisson's ratio versus longitudinal strain curve appears in Figure (9). This curve was abstracted from Nadai[12]. The current average Poisson's ratio value was computed by approximating this curve in a piecewise linear fashion over the longitudinal strain increment under consideration. Beyond 15,000 microinches/inch of longitudinal strain, the value at which the effective strain becomes equivalent to the longitudinal strain, the Poisson's ratio value was taken to be 0.50.

Finally, the term pressure represents, essentially, the negative of the hydrostatic component of stress, or

$$P = -(\sigma_1+\sigma_2+\sigma_3)/3 \qquad (4)$$

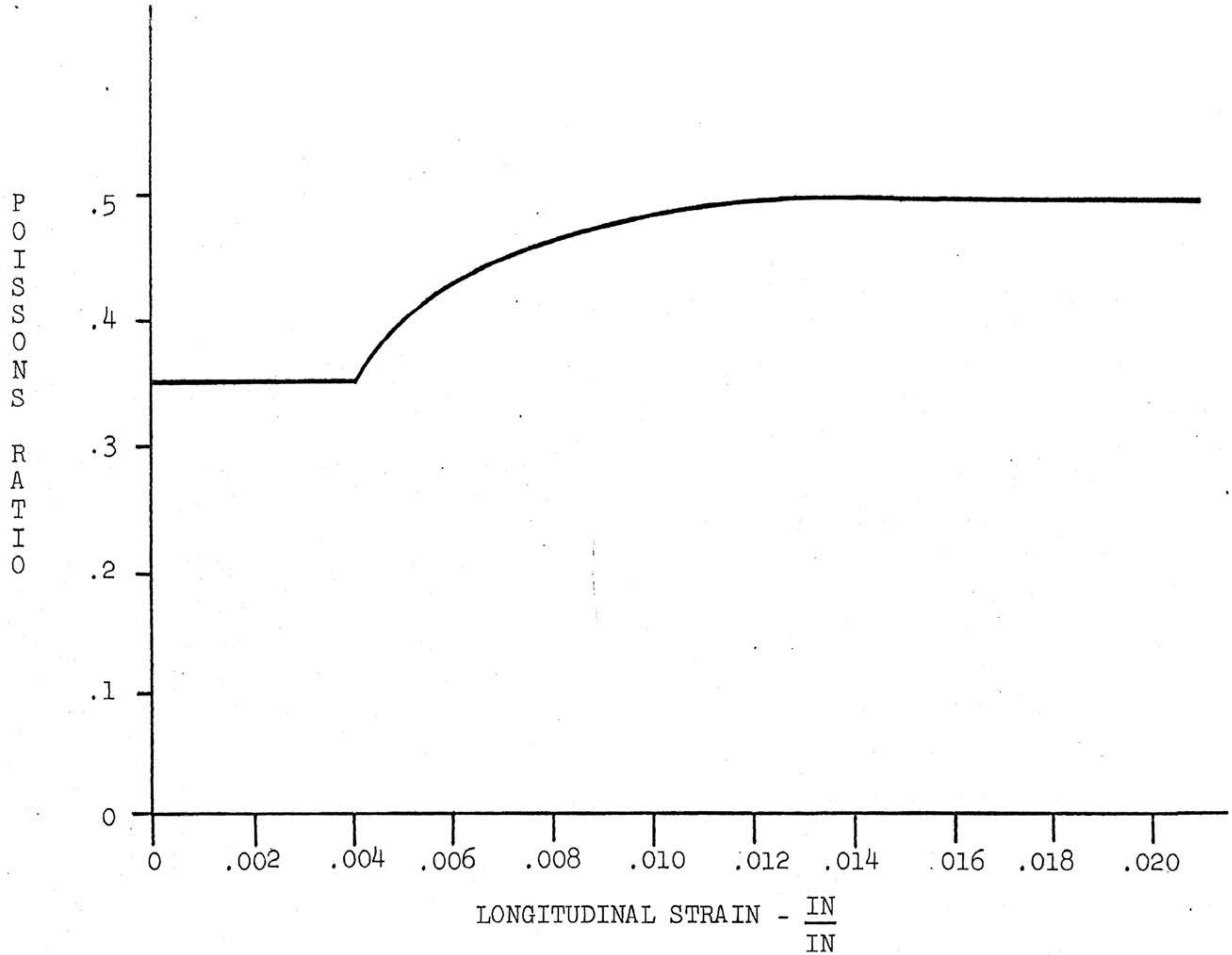

FIGURE (9) - POISSON'S RATIO versus LONGITUDINAL STRAIN

Figure (10), a plot of effective stress versus pressure, measured at yield, shows a slight enhancement of yield strength in compression as the pressure increases. However, the effective stress at yield in uniaxial tension (28,400 psi.) is considerably greater than the yield strengths achieved in compression, yet the pressure has been reduced to a negative value. This phenomenon is most unusual in a material and, in this case, results from the anisotropic properties generated by the extrusion process used to form the specimen bar stock. This is not a property of cast magnesium. For the above mentioned data points, yield was determined from a conventional plot of longitudinal stress versus longitudinal strain by using the 0.2 per-cent off-set method.

Figure (11), a plot of effective strain versus pressure at yield, shows a decrease in effective strain as the pressure increases. Once again, the effective strain at yield in uniaxial tension (6300 microinches/inch) is substantially greater than those experienced during the compression tests. This is not as incongruous as the previously mentioned observations concerning effective stress at yield, since the effective strain shows a tendency to decrease, rather than increase, as the pressure increases. However, the entire effect of decreasing effective strain with increasing pressure is, in itself, peculiar. Few, if any materials exhibit such tendencies. Since the slope of this curve is shallow, the possibility is strong that the increase in effective strain at yield achieved in the uniaxial tension test is not really a function of decreasing pressure at all; but is, instead, due to the fact that the specimen stock was extruded.

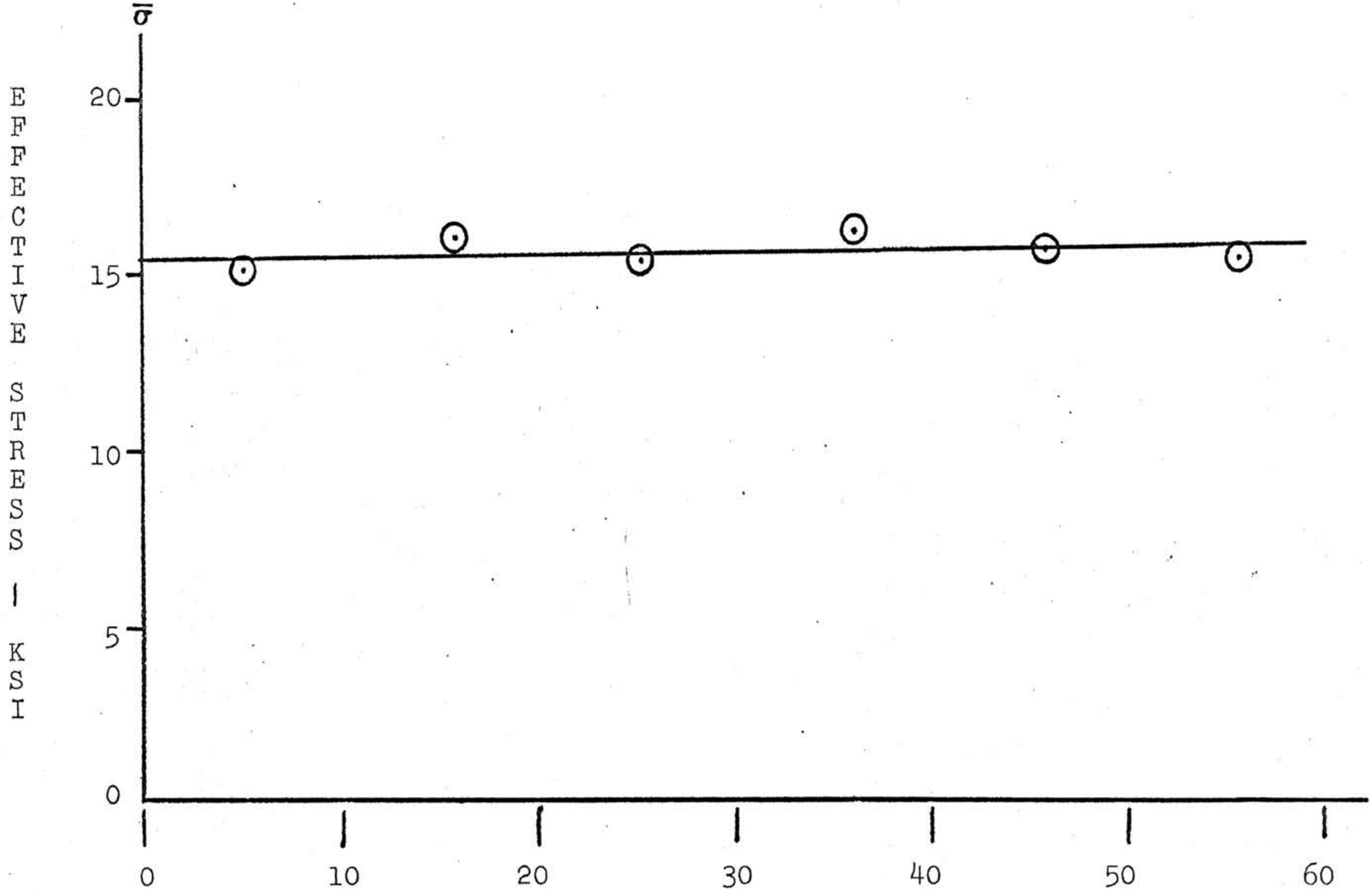

FIGURE (10) - EFFECTIVE STRESS AT YIELD versus PRESSURE

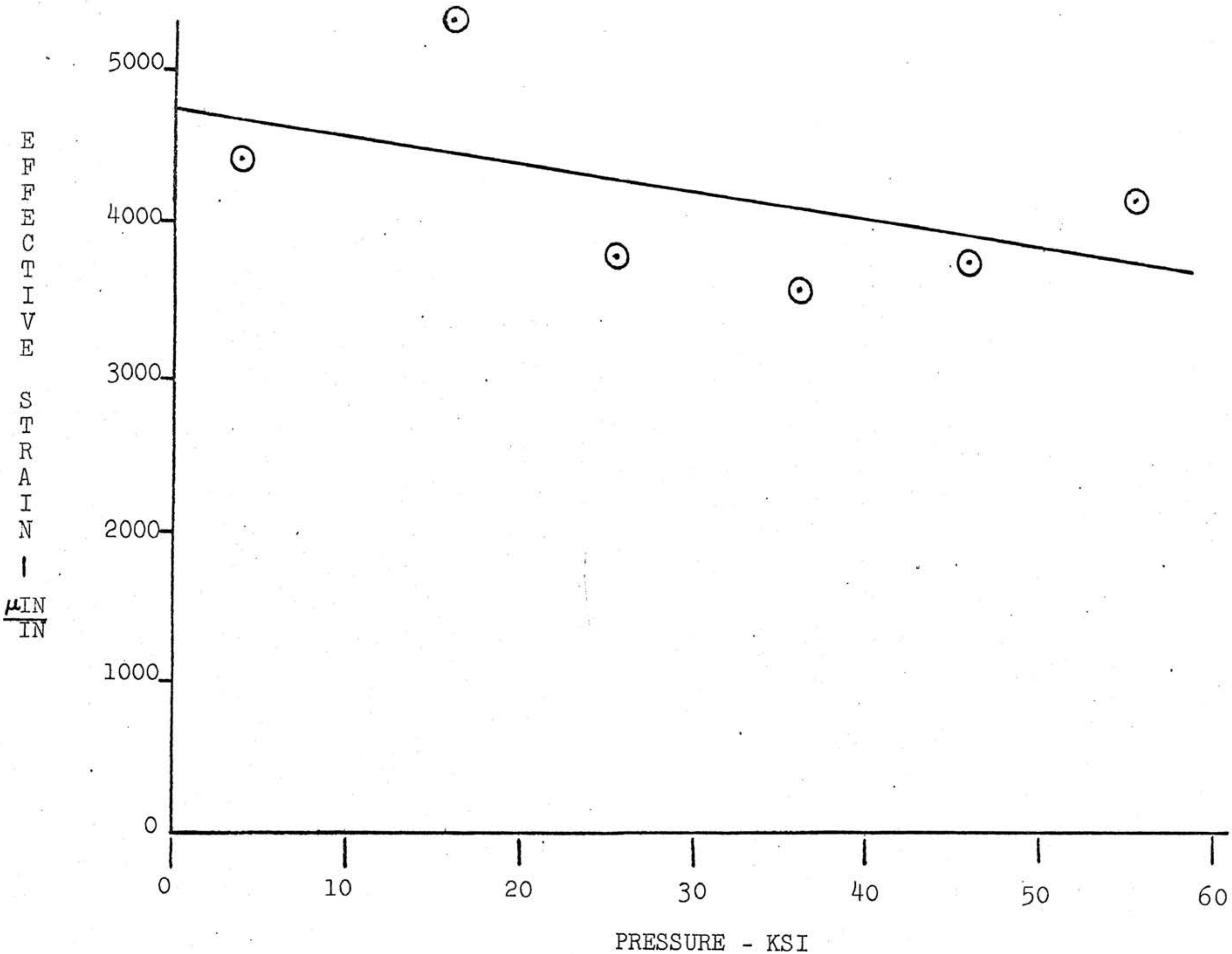

FIGURE (11) - EFFECTIVE STRAIN AT YIELD versus PRESSURE

Figures (12) and (13) describe, respectively, effective stress versus pressure and effective strain versus pressure at fracture. These plots are conventional in that this material appears to behave in a manner similar to a large group of engineering materials (for example, carbon steels). They show an increase in ductility and effective stress at fracture as the pressure is increased. The segments of these curves which appear in the compressive pressure region represent a line of work hardening shear fracture. It is common to discontinue this line at the effective stress or effective strain axis, and then continue into the tensile pressure region at a steeper slope. This steeper line is a line which represents work hardening tensile fracture points. The rationale for this is that the fracture mode should change from work hardening shear to work hardening tensile as the pressure is decreased into the tensile region. While one cannot deny that some materials behave in this manner, the author feels that the data available is not sufficient to warrant the extension of this hypothesis to all materials. As a result, the work hardening shear fracture lines have been extended linearly, into the region of tensile pressure to show another possibility.

More work is needed to define this transition point. A series of uniaxial tension tests in varying fluid pressure would suffice. Such tests would represent a loading path of slope -3 emanating from the point on the pressure axis corresponding to the fluid pressure.

A much more difficult problem arises when one considers the

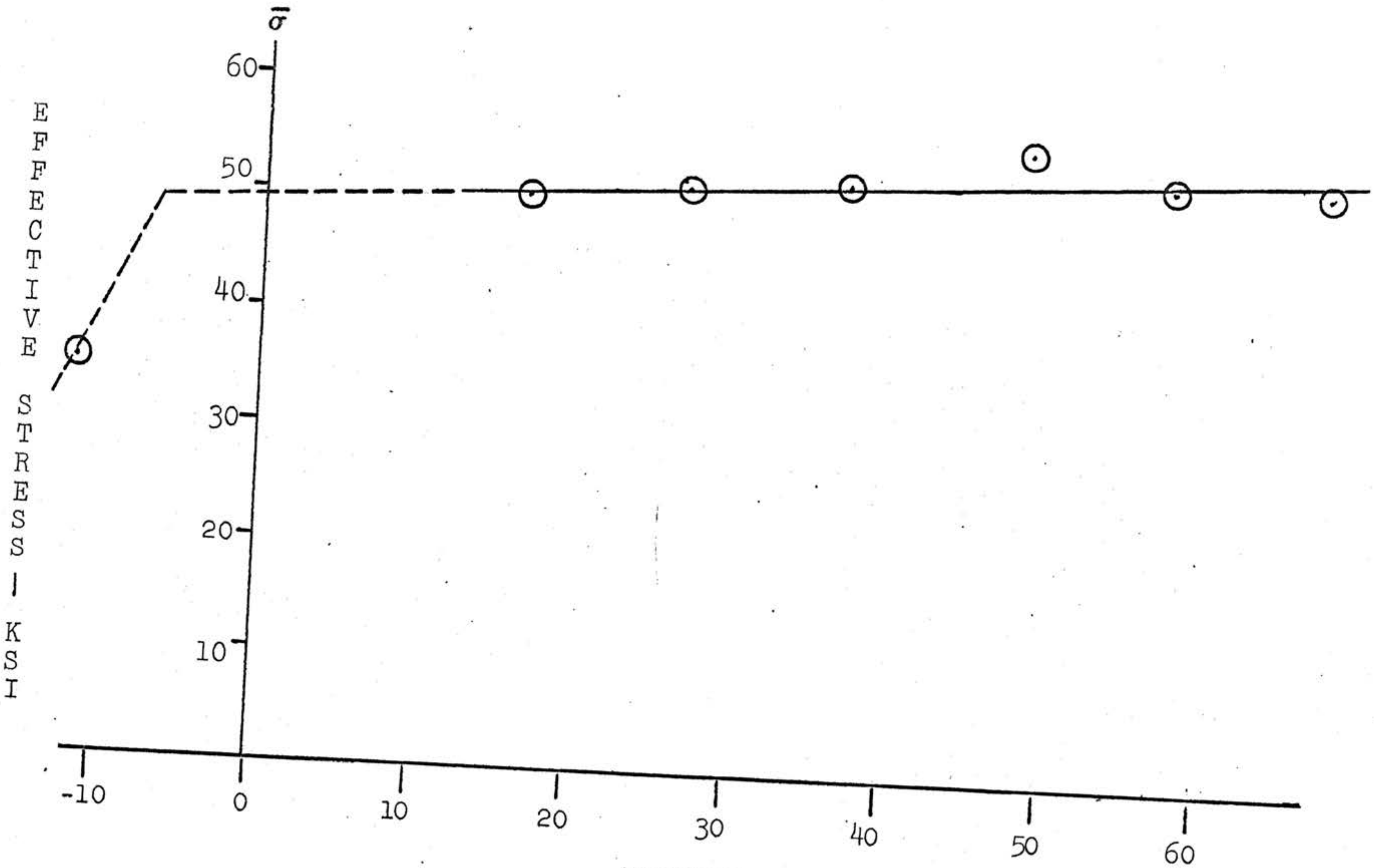

FIGURE (12) - EFFECTIVE STRESS AT FRACTURE versus PRESSURE

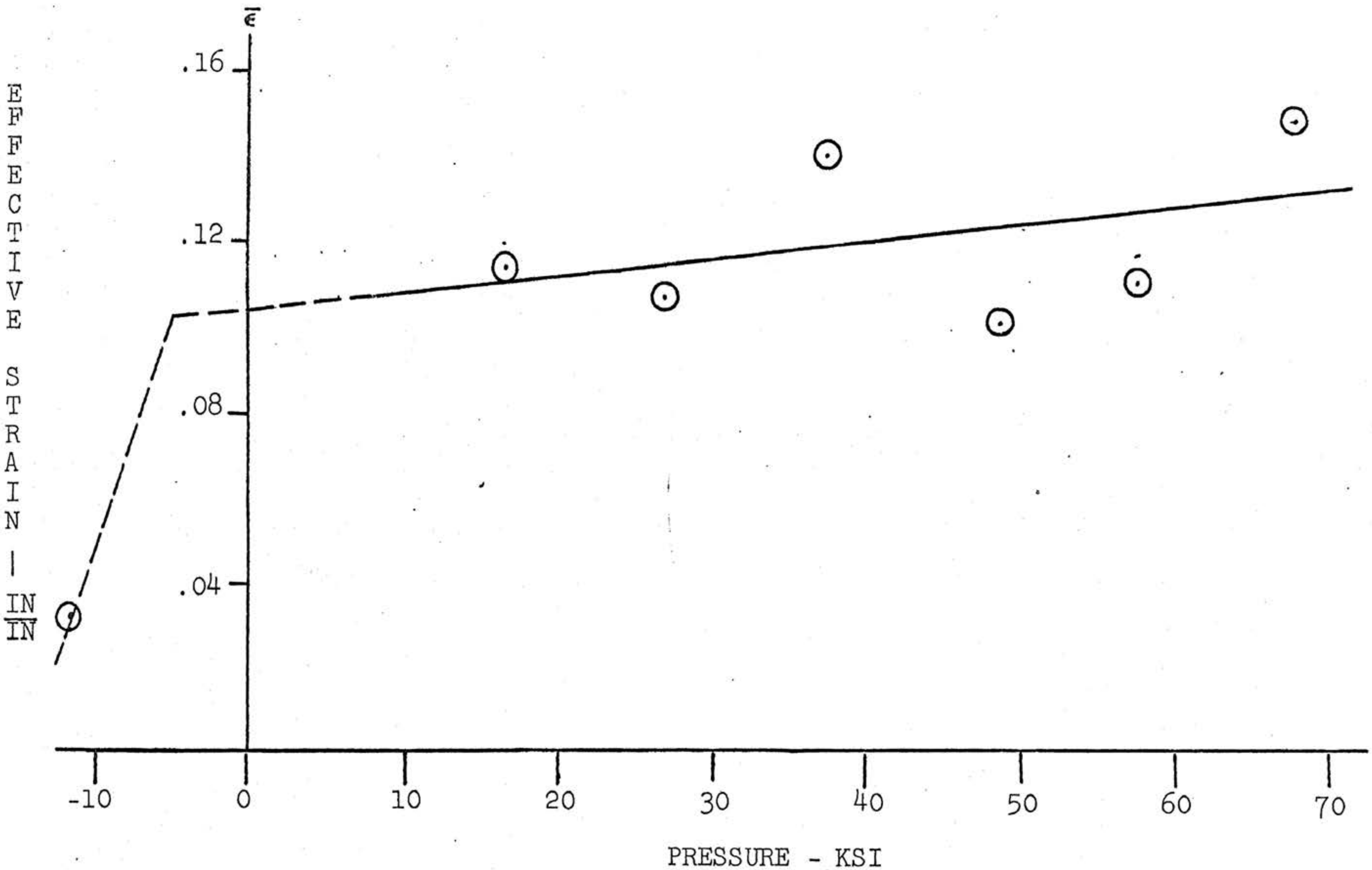

FIGURE (13) - EFFECTIVE STRAIN AT FRACTURE versus PRESSURE task of achieving data points on the work hardening tensile fracture line lower than that given by a uniaxial tension test run in the atmosphere. The shallowest negative slope on an effective stress versus pressure plot that can readily be obtained is -3/2. This can be accomplished in a bi-axial tension test. For bi-axial tension when both tensile stresses are of equal magnitude, σ,

$$\bar{\sigma} = \{(\sigma-\sigma)^2+(\sigma-0)^2+(0-\sigma)^2\}^{.5}/\sqrt{2} \tag{5}$$

$$\bar{\sigma} = \sigma \tag{6}$$

and the pressure is given by

$$P = -(\sigma+\sigma)/3 \tag{7}$$

This gives a loading path slope, $\bar{\sigma}/p$, of -3/2. By running such tests in varying fluid pressure environments, one can determine data points lying between lines emanating from the origin and having slopes of -3 and -3/2. This, however, does not complete the picture. For data points lying between the negative pressure axis and a line of -3/2 slope which intersects the pressure axis at the origin, some sort of a tri-axial tension test must be used. The existing tests, which generate a stress state in which all principal stresses are tensile, are of little value because the exact nature of the stress distributions is not accurately known. Such is the case in a tensile test of a circumferentially notched specimen. Since a good tri-axial tension test is not available, the behavior of a material at high tensile pressures is left almost totally to conjecture.

Finally, the results of the previous plots have been embodied in Figure (14) which is a three dimensional yield and fracture model based on the parameters of effective stress, effective strain, and pressure. Figure (15), a yield and fracture model for brass developed from Hu's data[13] by Davis[14], is included to illustrate a model constructed for a typically ductile, isotropic material. The purpose of these models is to show, for a virgin material, what yield and fracture phenomena will be experienced as any particular loading path is transversed. A loading path is essentially traced out by a point moving on the model surfaces. When the loading path hits a yield line, the material yields, and when the loading path hits a fracture line, fracture occurs.

In Figure (14), the line running from the origin to point (A) on the work hardening shear fracture line represents the intersection of the zero pressure plane and the elastic and plastic surfaces. This line delineates the portions of the elastic and plastic surfaces which lie in the tensile and compressive pressure regions; beyond this, it is of no physical significance. The portion of the model that exists in the region of tensile pressure is purely speculative since only one loading path was investigated in this area. As in the previous two plots, the yield and work hardening shear fracture lines have been extended, linearly, into the tensile pressure area. Point (B) marks the point on the fracture edge below which intrinsic brittle fracture can occur without previous yielding. Observation of the effective stress versus effective strain plots made for the compression test runs indicates that the contour of the elasto-

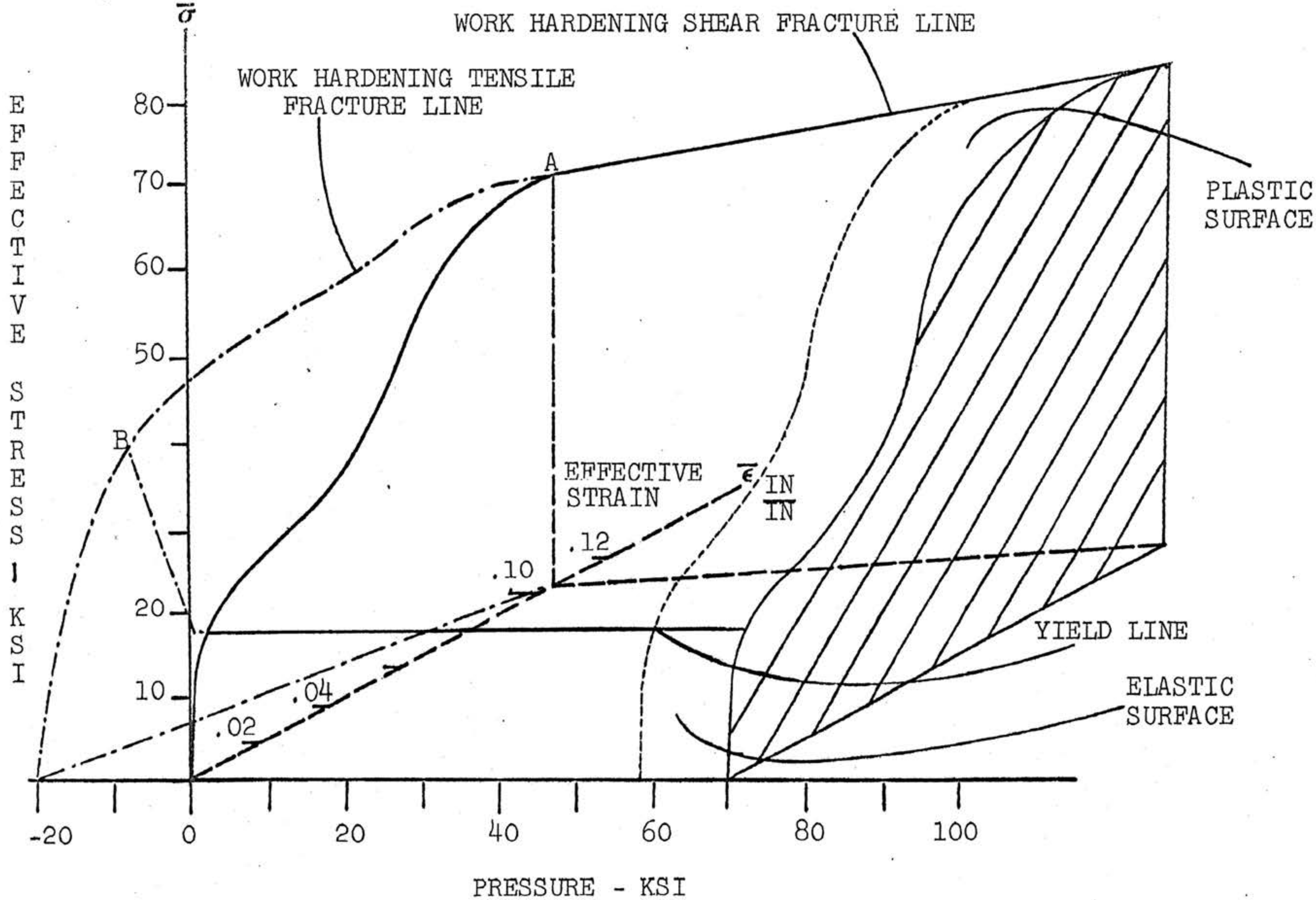

FIGURE (14) - THREE DIMENSIONAL YIELD AND FRACTURE MODEL FOR MAGNESIUM

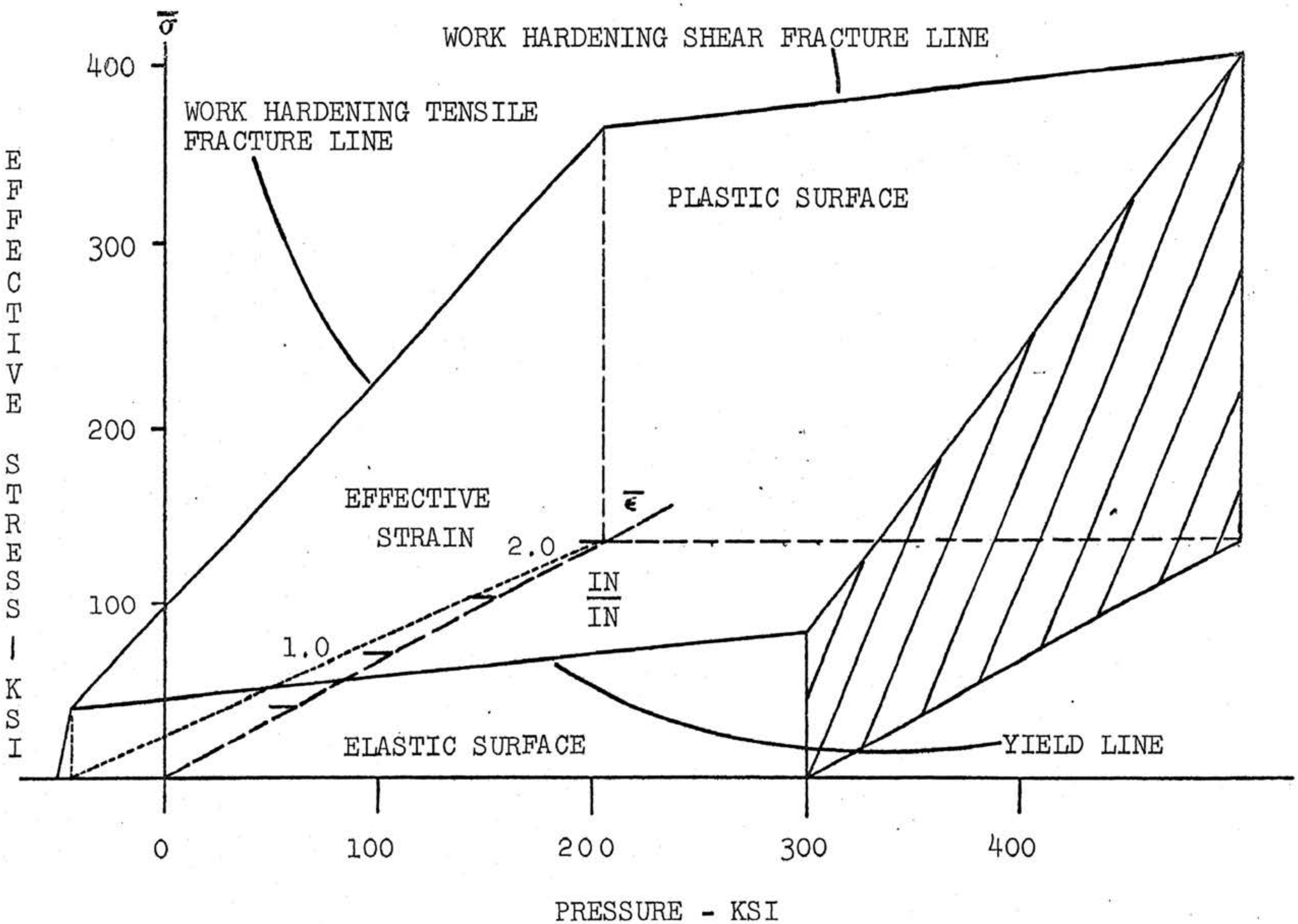

FIGURE (15) - THREE DIMENSIONAL YIELD AND FRACTURE MODEL FOR BRASS plastic surface does not significantly change in the compressive pressure region.

In addition to the tests described previously which are needed to define the tensile pressure section of the model, compression tests must be run at higher fluid pressure environments to determine what trends, if any, are shown in the direction of infinite ductility. For the test runs conducted in compression, no changes were noted in the fracture mode. The broken specimens are shown in Figure (16). They are oriented in the figure from left to right in order of increasing fluid environment pressure. Although the picture does not so indicate, the fracture surfaces were similar in appearance on all specimens.

In conclusion, one can say that the postulated model provides a good illustration of the properties which extruded AZ31B-F magnesium alloy exhibits under compressive pressures. The model describing material properties under tensile pressures, although crude, may well give a reasonably accurate description under such stress states.

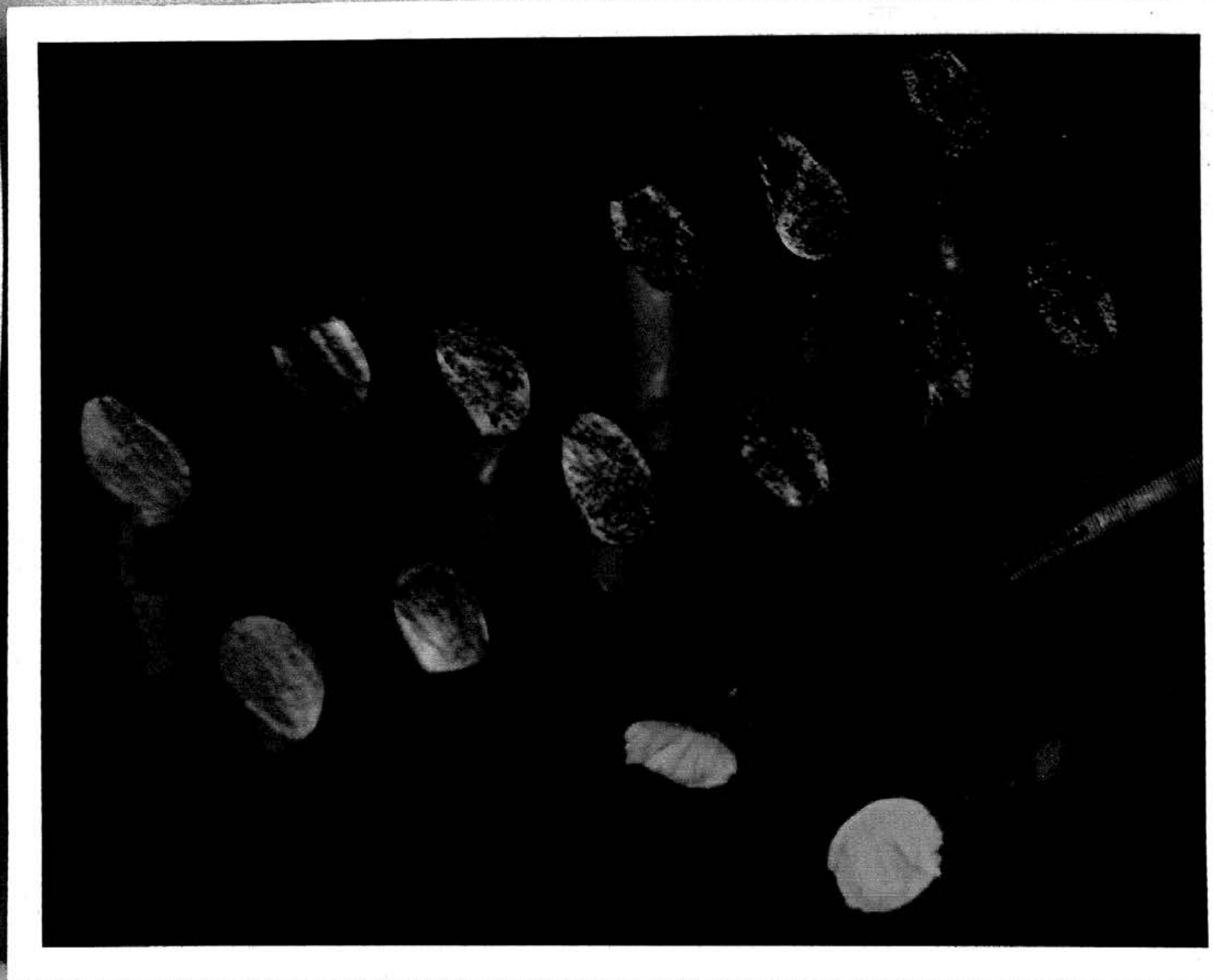

FIGURE (16) - FRACTURED SPECIMENS

TENSION TEST DATA

LOAD (POUNDS)	LONGITUDINAL STRAIN (EXTENSO-METER) (MICROINCHES/INCH)	LONGITUDINAL STRAIN (STRAIN GAUGE) (MICROINCHES/INCH)
0	0	0
1,000	125	333
2,000	300	531
3,000	450	711
4,000	625	900
5,000	800	1080
6,000	950	1260
7,000	1150	1449
8,000	1275	1647
9,000	1500	1859
10,000	1725	2079
11,000	1950	2340
12,000	2250	2682
13,000	2700	3164
14,000	3225	3663
15,000	3650	4140
16,000	4000	4306
17,000	4250	4590
18,000	4650	4860
19,000	5000	5161
20,000	5300	5715
21,000	5750	5895
22,000	6500	6534
23,000	7400	7380
24,000	8700	8550
25,000	10750	10332
26,000	13400	12667
27,000	16750	15660
28,000	24500	22473
28,500	28000	25560
29,000	32750	29745
29,500	38000	31896

COMPRESSION TEST DATA

(ATMOSPHERIC ENVIRONMENT)

LOAD (POUNDS)	LONGITUDINAL STRAIN (MICROINCHES/INCH) (EXTENSO-METER)	LONGITUDINAL STRAIN (MICROINCHES/INCH) (STRAIN GAUGE)
0	0	0
1,000	1170	779
3,000	2000	1116
4,000	2170	1310
5,000	2500	1500
6,000	2730	1679
7,000	3200	1881
8,000	3430	2095
9,000	3830	2317
10,000	4266	2430
11,000	4667	2700
12,000	6000	4325
13,000	8830	8100
14,000	15300	16110
15,000	22300	23814
16,000	28670	29871
17,000	35000	35640
18,000	40000	40010
19,000	44330	43686
21,000	52000	50616
22,000	55300	53550
23,000	58300	56219
24,000	60670	58815
25,000	63670	61484
26,000	66000	63716
27,000	68300	66029
28,000	70300	68220
29,000	72500	70438
30,000	74670	72612
31,000	76670	74511
32,000	78330	76289
33,000	80670	78026
34,000	82670	80042
35,000	84300	82310
36,000	86670	84344
37,000	88670	86432
38,000	91000	88691
39,500	93670	92399
41,000	98300	96350
42,000	101000	99865
43,000	105300	104306
44,000	109300	109725
44,800	-	120033

COMPRESSION TEST DATA

(10,000 PSI. FLUID ENVIRONMENT)

LOAD (POUNDS)	LONGITUDINAL STRAIN (MICROINCHES/INCH)
4,600	0
5,000	279
6,000	504
7,000	774
8,000	968
9,000	1134
10,000	1350
11,000	1521
12,000	1692
13,000	1881
14,000	2088
15,000	2354
16,000	2560
17,000	3100
18,000	5600
19,000	11025
20,000	18054
21,000	23598
22,000	28652
23,000	34367
24,000	38664
25,000	42786
26,000	45954
27,000	49050
28,000	52020
29,000	53995
30,000	57105
31,000	59454
32,000	62010
33,000	63630
34,000	65493
35,000	67401
36,000	69462
37,000	71577
38,000	73440
39,000	75375
40,000	77202
41,000	79245
42,000	81450
43,000	83781
44,000	86153
45,000	88506
46,000	91026
47,000	93510
48,000	97110
49,000	101070
50,000	105390
49,600	107879

COMPRESSION TEST DATA

(20,000 PSI. FLUID ENVIRONMENT)

LOAD (POUNDS)	LONGITUDINAL STRAIN (MICROINCHES/INCH)
8,500	0
9,600	207
10,000	270
11,000	468
12,000	621
13,000	765
14,000	918
15,000	1089
16,000	1269
17,000	1470
18,000	1690
19,000	1990
20,000	2450
21,000	3890
22,000	8300
23,000	15800
24,000	23697
25,000	30015
27,000	39114
28,500	44775
29,000	46260
30,000	49500
31,000	52425
32,000	54954
33,000	57618
34,000	59976
35,000	62055
36,000	64229
37,000	66300
38,000	68293
39,000	70074
40,000	72081
42,000	75870
43,000	77877
44,000	79965
45,000	81990
46,000	84150
47,000	86805
48,500	90495
49,000	91800
50,000	94690
52,000	102285
53,000	107001
54,000	114570
55,000	123525
55,400	140625

COMPRESSION TEST DATA

(30,000 PSI. FLUID ENVIRONMENT)

LOAD (POUNDS)	LONGITUDINAL STRAIN (MICROINCHES/INCH)
12,000	0
16,000	324
18,000	630
20,000	990
21,000	1229
22,000	1400
23,000	1600
24,000	1860
25,000	2400
26,000	4150
27,000	7767
28,000	14180
29,000	20182
30,000	26289
31,000	31365
32,000	35550
33,000	39645
34,000	43038
35,000	46283
36,000	49500
37,000	51975
38,000	54730
39,000	56939
40,000	59018
41,000	61200
42,000	63113
43,000	65205
44,000	67050
45,000	68904
46,000	70704
47,000	72531
48,000	74277
49,000	76500
50,000	77904
51,000	79866
52,000	81518
53,000	83520
54,000	85770
55,000	87975
56,000	90378
57,000	93150
58,000	96165
59,000	99203
60,000	102285

COMPRESSION TEST DATA

(40,000 PSI. FLUID ENVIRONMENT)

LOAD (POUNDS)	LONGITUDINAL STRAIN (MICROINCHES/INCH)
17,000	0
19,000	135
20,000	315
21,000	491
22,000	666
24,000	1035
25,000	1242
26,000	1427
27,000	1638
28,000	1917
29,000	2360
30,000	3470
31,000	7858
32,000	13815
33,000	19665
34,000	25461
35,000	30416
36,000	35208
37,000	39150
38,000	42615
40,000	48600
41,000	50020
42,000	54900
43,000	56610
44,000	59063
45,000	61695
46,000	63765
47,000	65700
48,000	67590
50,000	71280
51,000	73080
52,000	74970
53,000	76835
54,000	78723
55,000	80703
56,000	82773
58,000	87300
59,000	89910
60,000	92394
61,000	95166
62,000	98262
63,000	101817
64,000	106335
65,000	110700
63,200	117540

COMPRESSION TEST DATA

(50,000 PSI. FLUID ENVIRONMENT)

LOAD (POUNDS)	LONGITUDINAL STRAIN (MICROINCHES/INCH)
22,200	0
24,000	320
25,000	495
26,000	720
27,000	918
28,000	1125
30,000	1512
31,000	1730
32,000	1980
33,000	2250
34,000	2490
35,000	3550
36,000	6791
37,000	12630
38,000	18400
39,000	24030
40,000	28728
41,000	33318
42,000	38763
43,000	42030
44,000	45153
45,000	48285
46,000	52668
47,000	56403
48,000	59553
49,000	61938
50,000	63513
51,000	65178
52,000	66960
54,000	70830
55,000	72531
56,000	74547
57,000	76460
58,000	78390
59,000	80388
60,000	82296
61,000	84600
62,000	86850
64,000	91728
65,000	94608
66,000	97893
67,000	101898
68,000	106803
69,000	114228
70,000	126000
70,900	148653

BIBLIOGRAPHY

1. COOK, G. (1934) Effects of Fluid Pressure on the Permanent Deformation of Metals by Shear. London, Inst. of Civil Engineers, 8 p.

2. BRIDGEMAN, P. W. (1952) Large Plastic Flow and Fracture. New York, McGraw-Hill, 355 p.

3. BRIDGEMAN, P. W. (1934) Compressibility of Selected Crystals. Proceed. of the Amer. Acad. of Arts and Sci., Vol. 66, p. 261-262.

4. ZEITLIN, A. (1964) Annotated Bibliography on High-Pressure Technology. Washington, D. C., Butterworths, 290 p.

5. BUNDY, F. P., HIBBARD, W. R., and STRONG, H. M. (1960) Progress in Very High Pressure Research. New York, Wiley, 313 p.

6. BRADLEY, R. S. (1966) Advances in High Pressure Research, Vol. I. New York, Academic Press.

7. GIARDINI, A. A., and LLOYD, E. C. (1963) High Pressure Measurement. Washington, D. C., Butterworths.

8. Proceedings of the International Conf. on the Phys. of Solids at High Pressures (1965). Published by the Conf.

9. HU, L. W. (1965) A Triaxial Experiment on Yield Condition in Plasticity. Air Force Office of Scientific Research Sci. Report no. 65-0313.

10. GORDON, R. B., and TIEN, J. K., (1964) Use of Electrical Resistance Strain Gages Under Hydrostatic Pressure. ASME Publication 64-WA/PT-20.

11. WOLF, R. (1968) Personal communication.

12. NADAI, A. (1963) Theory of Flow and Fracture of Solids, Vol. II. New York, McGraw-Hill, p. 33-34.

13. HU, L. W. (1958) Determination of the Plastic Stress-Strain Relations for Nittany No. 2 Brass under Hydrostatic Pressure. Proc. 3rd. U. S. National Congress of Applied Mechanics.

14. DAVIS, R. L. (1966) Pressure Dependent Yield and Fracture Models from Available Experimental Data. Pittsburg, Research Session, Metal Forming, SESA Annual Meeting.

VITA

The author was born on December 13, 1943, in WilkesBarre, Pennsylvania. He received his primary and secondary education in Dallas, Pennsylvania. He was awarded a Bachelor of Science Degree in Mechanical Engineering by the University of Maryland in June, 1965.

Upon completion of his undergraduate work, he accepted a position in the United States Department of the Navy Bureau of Naval Weapons and held that position until entering graduate school.

He has been enrolled in the Graduate School of the University of Missouri at Rolla since September, 1966, and has held a Graduate Teaching Assistantship, from that date, while pursuing the degree Master of Science in Engineering Mechanics.